Colloid Polym Sci (2008) 286:683–689
DOI 10.1007/s00396-007-1819-1

ORIGINAL CONTRIBUTION

Composites comprising CdS nanoparticles and poly(ethylene oxide): optical properties and influence of the nanofiller content on the thermal behaviour of the host matrix

T. Radhakrishnan · M. K. Georges · P. Sreekumari Nair · A.S. Luyt · V. Djoković

Received: 20 June 2007 / Revised: 20 November 2007 / Accepted: 29 November 2007 / Published online: 19 December 2007

Abstract Tri-*n*-octylphosphine oxide-capped CdS nanoparticles were synthesized with the cadmium(II) complex of thiocarbohydrazide as a precursor. Nanocomposites were prepared by mixing a toluene solution of poly(ethylene oxide) (PEO) and the obtained CdS nanoparticles. The ultraviolet-visible spectroscopy measurements showed a blue shift of the onset of optical absorption, compared to bulk CdS, which confirmed the presence of nanostructured CdS. A transmission electron microscopy micrograph of the nanocomposite depicted that the nanoparticles are well dispersed in the PEO matrix. Differential scanning calorimetry analysis revealed hindered crystallization of PEO in the presence of CdS nanoparticles. It was also found that increasing the nanoparticle content led to the shift of the onset of decomposition of the matrix towards higher temperature.

T. Radhakrishnan (✉) · M. K. Georges
Department of Chemistry, University of Toronto at Mississauga,
Mississauga, Ontario, Canada
e-mail: tradhakr@utm.utoronto.ca

P. Sreekumari Nair
Department of Chemistry Lash-Miller Chemical Laboratories,
University of Toronto,
Toronto, Ontario, Canada M5S 3H6

A. Luyt · V. Djoković
Department of Chemistry,
University of the Free State (Qwa Qwa Campus),
Private Bag X13,
Phuthaditjhaba 9866, South Africa

V. Djoković (✉)
Institut of Nuclear Sciences "Vinča",
P.O. Box 522, 11001 Belgrade, Serbia and Montenegro
e-mail: djokovic@vin.bg.ac.yu

Keywords CdS · Nanoparticle · Nanocomposite · TOPO · PEO · Crystallization

Introduction

There is a high level of interest in the preparation and characterization of semiconductor-polymer nanocomposites due to a broad range of potential applications of these materials [1–28]. Semiconductor nanoparticles exhibit size-dependent physical properties stemming from quantum confinement effects, which can be successfully exploited by their incorporation into the polymer matrix [1]. Using polymers as the matrix for nanoparticles (not necessarily semiconductor) has several advantages. Besides well-known polymer properties, such as long-term dimensional stability and ease of processing into desired bulk shapes, which are important from an engineering point of view, the matrix may also play a role in controlling the nanocrystal growth [9–11]. On the other hand, because nanoparticles possess large surface areas relative to their volumes, they can affect the host polymer to a large extent, which sometimes leads to the interesting hybrid properties [19–21, 26].

CdS is a II-VI semiconductor which absorbs in the visible part of the electromagnetic spectrum (bulk band gap of 2.4 eV). Because of their characteristic optical properties, that are size tunable at particle diameters lower or comparable to the diameter of the bulk exciton (60 Å), CdS nanoparticles find possible applications as optical switches, sensors, electro-luminescent devices [29] and biomedical tags [30]. Since some of these applications can be facilitated by introducing nanoparticles into polymers, a number of studies on CdS nanocomposites emerged recently [1–23]. They presented different methods for the preparation of the nanocomposites that can be roughly

divided into in situ reactions, where the particles are generated from the respective precursors in the presence of the matrix polymer, and ex situ reactions, where the nanoparticles are synthesized and then mixed with the polymer. In situ methods are based on the concept of using the polymer matrix to partially reduce diffusion of the particles to control the growth and dispersion of the nanoparticles formed. Furthermore, functional groups of the polymer and especially the co-polymer matrices can be used to assist in the synthesis of CdS nanocrystals. Several authors exploited this idea in the fabrication of homopolymer- [5, 9, 11, 12] and copolymer-CdS [8, 10, 14] nanocomposites. In a previous study, we used this approach in the preparation of polystyrene-co-maleic acid (PS-co-MAc)-CdS nanocomposites [21]. Although in situ methods enable good dispersion of the nanoparticles into the polymer matrix, the size distribution of the nanoparticles can be better controlled if they are synthesized separately and then mixed with polymer. In fact, by using highly developed methods of surface modification in colloidal chemistry, it is possible to obtain semiconductor nanoparticles with well defined size and shape. For example, Tamborra et al. [7] prepared blue-luminescent PS-CdS and Poly(methylmethacrylate) (PMMA)-CdS nanocomposites by solution mixing of previously obtained oleic acid capped CdS nanoparticles and the corresponding polymers. A similar method was used by Nedeljković and co-workers [20] in the fabrication of PS-CdS nanocomposite films. They first prepared a CdS water colloid, then extracted the CdS nanoparticles in an organic solvent by using suitable surfactants, and finally mixed the CdS organic colloid with the polymer. In this study, we also used solution mixing to prepare the nanocomposites of polyethylene oxide (PEO) and tri-*n*-octylphosphine oxide (TOPO)-capped CdS nanoparticles. Phosphine derivatives, especially tri-*n*-octylphosphine oxide, were extensively used in the synthesis of high-quality CdE (E=Se, S, Te) nanocrystals (particles and rods) [31–34]. Usually, the starting cadmium precursor in the preparation of the above-mentioned semiconductors were either dimethyl cadmium [$Cd(CH_3)_2$] or newly introduced CdO [33, 34]. Recently, we synthesized TOPO-capped CdS nanorods [35] using a procedure based on the thermolysis reaction of a cadmium(II) complex of thiosemicarbazide [$Cd(H_2NCSNHNH_2)_2Cl_2$]. In this paper, we present a novel precursor, the cadmium(II) complex thiocarbohydrazide [$Cd(H_2NHNCSNHNH_2)_2(CH_3COO)_2$], as a source for the preparation of nanostructured CdS. However, because of the slightly different structure of the latter Cd complex, its thermolysis resulted in the formation of spherical CdS nanoparticles instead of rods. The properties of the obtained TOPO-capped CdS nanoparticles were first studied using optical and structural techniques, and thereafter, they were introduced into a PEO matrix via solution mixing.

The polyether polymer, PEO, is an important material for electrochemical [36] and biomedical [37] applications. So far, various nanostructured fillers were used to modify and improve its properties [22, 38–44]. A recent review of Caseri [45] reports that the composite of PEO and nanostructured PbS can be used in the fabrication of high-refractive-index polymer materials. Some of the mentioned studies [38, 39, 42, 43] show that the nanofiller, depending on its type, structure and composition, can induce changes in thermal properties (melting, crystallization etc.) of the PEO matrix. Taking into account the former remark, we decided that the objective of the present study should be twofold: first, to investigate the optical properties of the prepared CdS nanoparticles (isolated and in the PEO matrix) and second, to establish the possible influence of the nanoparticles on the thermal properties of the host polymer.

Experimental

Preparation of the CdS nanoparticles

CdS nanoparticles were obtained using the cadmium(II) complex of thiocarbohydrazide $Cd(H_2NHNCSNHNH_2)_2(CH_3COO)_2$ as a precursor for the thermolysis reaction in TOPO. The method is similar to the procedure suggested in our previous study [35] where a thiosemicarbazide complex of cadmium [$Cd(H_2NCSNHNH_2)_2Cl_2$] was used for the preparation of CdS nanorods. To prepare Cd $(H_2NHNCSNHNH_2)_2(CH_3COO)_2$, cadmium acetate and thiocarbohydrazide (1:2 mol ratio) were refluxed in ethanol for 3 h. The white solid product formed was filtered, washed with ethanol and dried. To synthesize CdS nanoparticles, about 1 g of precursor complex was dispersed in 10 ml of tri-*n*-octylphosphine and injected into hot (225 °C) TOPO. The temperature was increased to 290 °C and maintained at this level for 45 min. For absorption measurements, about 1 ml of the solution was withdrawn at 5, 10, 20 and 30-min time intervals. Methanol was added to precipitate the CdS, which was centrifuged, isolated and dried. After 45 min, the heating was stopped, and the rest of the solution was cooled to 70 °C. The CdS was isolated by using the same procedure. The CdS nanoparticles obtained at the end of the reaction procedure were further dissolved in toluene and used for fabrication of the nanocomposite.

Preparation of the PEO-CdS nanocomposites

To prepare the nanocomposites, 10 ml of toluene was first added in glass beakers containing 0.5, 1.5 and 2.0 g of PEO (Aldrich, Mw=100,000 $g \cdot mol^{-1}$), respectively. Thereafter,

10 ml of toluene solution of CdS nanoparticles was added in each beaker, slowly, with heating and vigorous stirring. PEO got dissolved after approximately 20 min, and turbid, yellow solutions were formed. The solutions were poured on glass plates and left to dry in air. Yellow nanocomposite materials with different amount of inorganic phase were obtained after solvent evaporation. Pure PEO film was prepared in a similar way.

Apparatus

The morphology and dispersion of the CdS nanoparticles before and after introduction in the PEO matrix were investigated by transmission electron microscopy (Phillps CM100 instrument). The TOPO-capped nanoparticles obtained at the end of the isolation procedure were deposited on a carbon-coated thin-bar copper grid using a fine pipette. A similar procedure was used in the preparation of the PEO-CdS sample, but the nanocomposite was dissolved in water and a 200 mesh formvar (amorphous polymer) coated Athene copper grid (Agar Scientific) was used instead. The samples were left to dry in air before they were transferred to the transmission electron microscope (TEM) chamber. The operating voltage during TEM analysis was 80 kV.

The X-ray diffraction (XRD) spectrum of the TOPO-capped CdS nanoparticles was obtained using a Philips PW3710 X-ray diffractometer (Cuα radiation, λ= 0.154 nm).

Absorption measurements were carried out by using a Perkin Elmer Lambda 5 UV-VIS spectrophotometer. The luminescence spectra of the PEO-CdS nanocomposite in water were recorded at a 400-nm excitation wavelength on a Perkin Elmer LS 3B spectrophotometer.

The crystallization and the melting behavior of PEO in the presence of CdS nanoparticles was investigated by means of differential scanning calorimetry (Perkin Elmer DSC7). The pure PEO and PEO-CdS nanocomposite samples (approximately 4 mg by weight) were heated from 20 to 90 °C, cooled to the same temperature using a 10 °C min^{-1} heating rate, and reheated. The presented curves were obtained in the second run. Up to seven samples of the pure matrix and each of the nanocomposite compositions were investigated, and the average values of the typical differential scanning calorimetry (DSC) parameters (melting and crystallization temperatures, enthalpies of melting end crystallization) are reported. Thermogravimetric analyses were carried out on a Perkin Elmer TGA7 in nitrogen atmosphere, and the temperature range was from 30 to 630 °C. The heating rate was 10 °C·min^{-1}. The content of the inorganic phase was determined as a residue at the end of the degradation process, and was found to be 1.8, 2.6 and 3.4 wt%, respectively.

Results and discussion

Optical properties

The ultraviolet-visible (UV-VIS) absorption spectra of TOPO-capped CdS nanoparticles, isolated from the reaction mixture at different time intervals, are shown in Fig. 1. All the spectra show a blue-shifted absorption onset with respect to the 517 nm of the bulk semiconductor, proving the presence of nanostructured CdS. A shift of the absorption onset towards lower energies also suggests that the growth of the nanoparticles can be controlled, to a certain extent, by reducing the time intervals at which they were isolated. The absorption onsets and the corresponding particle diameters (estimated using the Brus equation [46]) of the five CdS samples are presented in Table 1. It should also be noticed that, besides their larger sizes noted in Table 1, the samples isolated at longer intervals show much broader exciton peaks (Fig. 1). This means that longer isolation times do not just lead to nanoparticle crystal growth but also to the broadening of their size distribution [10]. Fig. 2 depicts typical absorption and emission spectra of the PEO-CdS nanocomposite. Except for the stronger absorption due to the presence of PEO, there are no significant differences between the spectrum of the nanocomposite and that of the CdS nanoparticles isolated at the end of the procedure (45 min curve in Fig. 1). The emission spectrum (Fig. 2) is dominated by a strong band-to-band recombination. A few low intensity bands on the orange–red side of the spectrum can be ascribed to the presence of sulfur vacancies at the surface of the nanocrystals, i.e. to the recombination at surface sites [16, 47, 48].

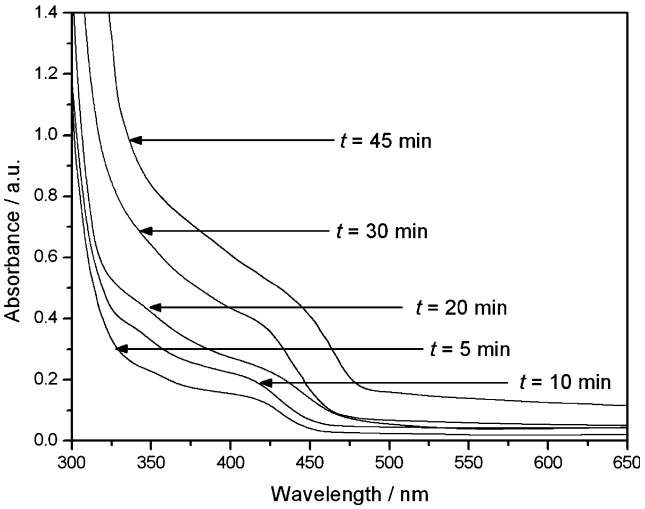

Fig. 1 UV-VIS absorption spectra of TOPO-capped CdS nanoparticles isolated at different time intervals

Table 1 Absorption edges and particle sizes of the CdS samples isolated at different time intervals

Sample no.	Time intervals (min)	Absorption edge (nm)	Particle size (nm)
1	5	460	4.4
2	10	462	4.5
3	20	463	4.5
4	30	478	5.1
5	45	484	5.3

Structural and morphological characterization

The TEM micrograph in Fig. 3 shows the CdS nanoparticles obtained at the end of the isolation procedure (after 45 min). Their sizes are in the range of 4–5 nm, which is in agreement with the particle diameter, d=4.2 nm (average size), estimated from the position of the exciton peak (456 nm) in Fig. 1 and the particle diameter that corresponds to the absorption onset (Table 1). The XRD spectrum of the TOPO-capped nanoparticles is presented in Fig. 4. The two observed peaks correspond to (111) and (220) of the cubic crystal phase of CdS.

Figure 5a depicts the TEM micrograph of the PEO-CdS nanocomposite. To make easier the distinction of the CdS particles from the darker (PEO) and lighter background (formvar amorphous polymer), few of them are circled and marked with arrows. The particles are relatively well dispersed in the matrix, although some clustering can also be noticed. The size distribution of the particles in Fig. 5a is shown in Fig. 5b. The distribution is narrow and asymmetric with the maximum at about 4 nm and the standard deviation of σ_N=1.6 nm, which also corresponds well with the value of d=4.2 nm obtained from the positions of the exciton peaks in Figs. 1 (45 min curve) and 2. It is worth mentioning that, compared to our previous study [35] where the decomposition of the thiosemicarbazide complex of cadmium [Cd(H2NCSNHNH2)2Cl2] induced the formation of CdS nanorods, in the present case, a relatively similar cadmium complex of thiocarbohydrazide Cd $(H_2NHNCSNHNH_2)_2(CH_3COO)_2$ leads to the formation of spherical particles. Thermogravimetric analyses (TGA) measurements (not shown) also revealed that both complexes have a similar decomposition route. That is why we believe that the different shapes of the obtained nanostructured CdS are rather the consequence of a slightly different position of the S atom in the thiosemicarbazide and thiocarbohydrazide than of the presence of different anions in the two precursors.

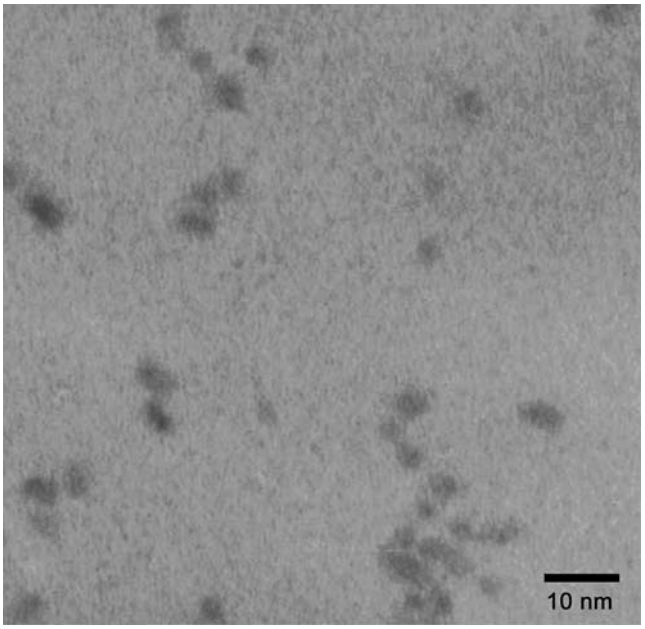

Fig. 3 TEM micrograph of TOPO-capped CdS nanoparticles isolated from the reaction mixture at the end of the procedure (after 45 min)

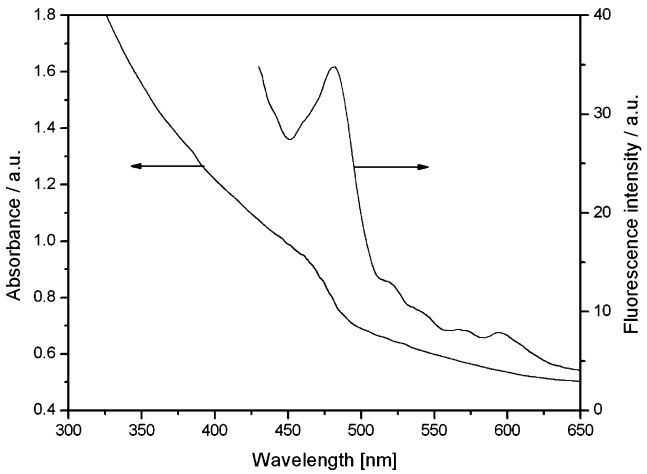

Fig. 2 Typical absorption and emission spectra of a PEO-CdS nanocomposite. The absorption spectrum was recorded with the sample in water solution. The emission spectrum of solid nanocomposite was obtained at an excitation wavelength of 380 nm

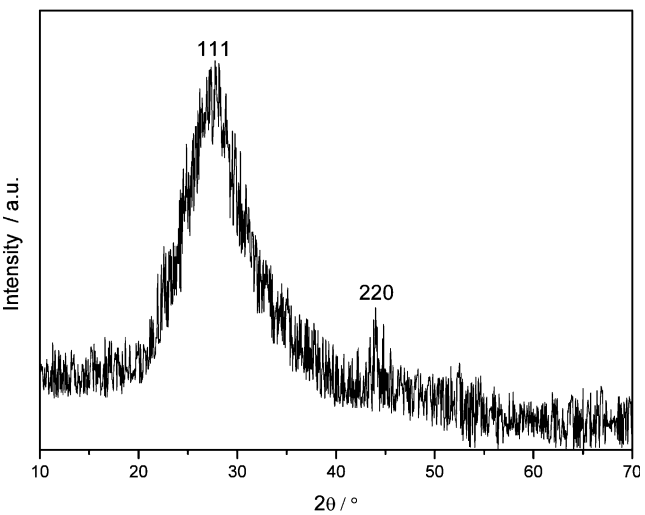

Fig. 4 XRD spectrum of TOPO-capped CdS nanoparticles

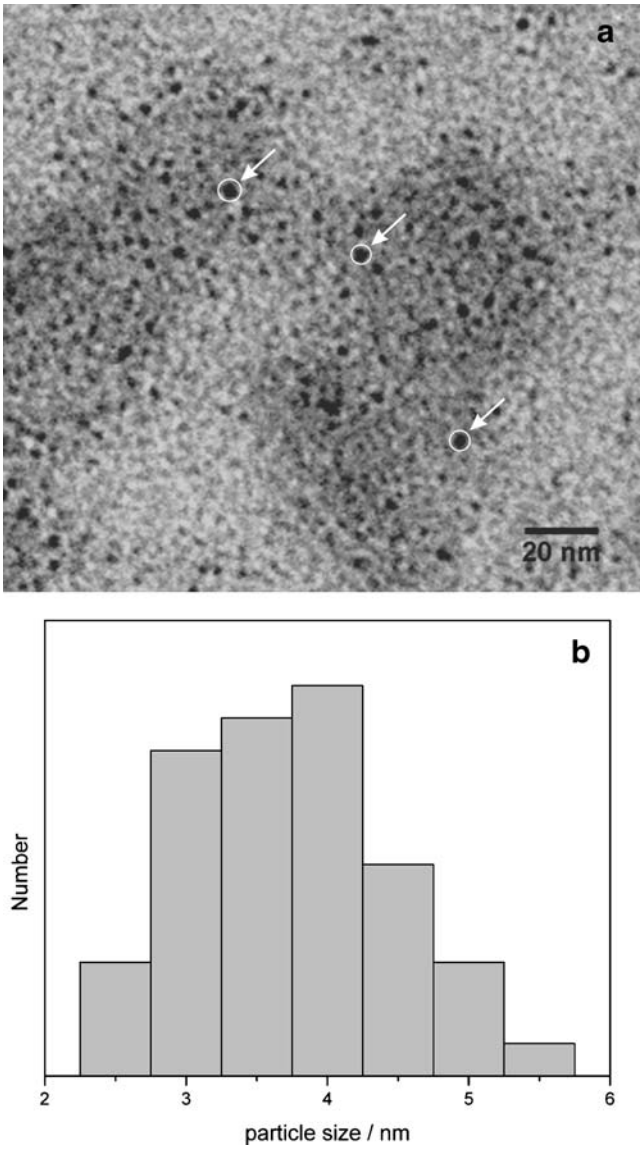

Fig. 5 **a** TEM micrograph of a PEO-CdS nanocomposite; **b** particle size distribution histogram of the CdS nanoparticles in the PEO matrix. The number of particles counted for the histogram was 100

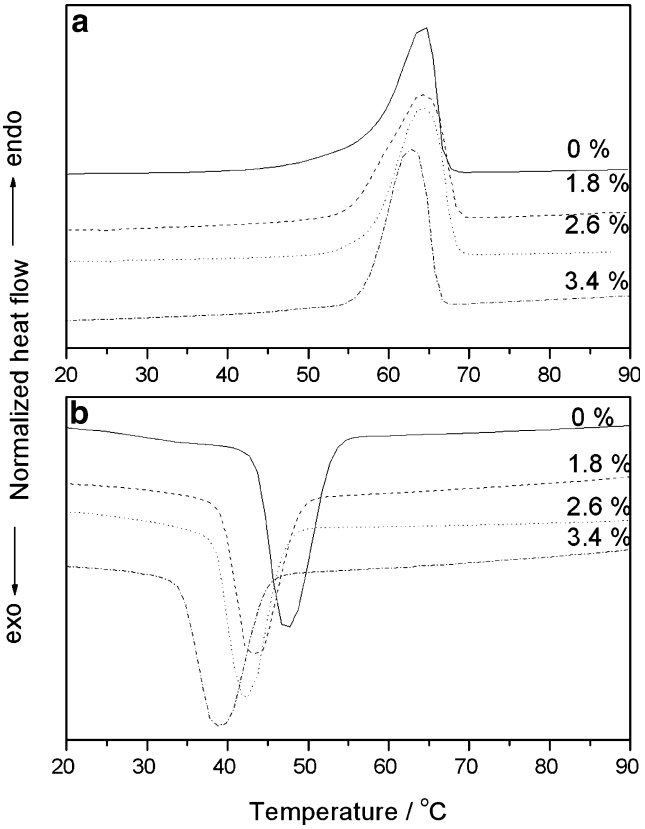

Fig. 6 DSC endothermic (**a**) and exothermic (**b**) curves of pure PEO and PEO-CdS nanocomposites with various nanoparticle contents. Heating and cooling rates were 10 °C min^{-1}

Thermal properties

The DSC heating and cooling curves of pure PEO and PEO-CdS nanocomposites are shown in Fig. 6. It can be seen that the melting peak temperature is not significantly affected by the presence of CdS nanoparticles (except for the sample with 3.4% of inorganic phase). In contrast, the peak temperature of crystallization gradually decreases with increasing CdS content. Obviously, a higher degree of undercooling is necessary for crystallization of the nanocomposite. It should be noted that the enthalpies of melting and crystallization of the nanocomposite samples are slightly lower than those of the pure PEO. Taking into account the standard deviations, the relative enthalpy changes are obviously less pronounced than the observed relative changes in crystallization temperatures (Table 2). This indicates that the introduction of nanoparticles hinders the crystallization of PEO but to a lesser extent influences its crystallinity. The present results are in agreement with results of Strawhecker and Manias [38] on the crystallization of PEO in the presence of montmorillonite (MMT)-Na^+ nanofillers. These authors also noticed that crystal growth of PEO slowed down in the vicinity of MMT filler. They argued that this effect was a result of the strong coordination of PEO macromolecules with small cations such as Na^+ and Li^+ [38]. The coordination promotes a "crown ether" type of backbone conformation, i.e. deviation from the helical conformation which is necessary for the packing of the chains into crystal lamellae. The former conclusion could be supported by molecular dynamic simulations at the interface between PEO and TiO_2 [49]. It was shown that the PEO oxygen atoms approach closest to the TiO_2 surface because they are attracted to Ti atoms with a positive partial charge of 1.4 e. As a result, a change in the distribution of the torsional C–O–C–C angles in interfacial PEO takes place. We believe that the conformational changes of the PEO chains are also responsible for the observed hindered crystallization in Fig. 6. Change in the helical conformation

Table 2 DSC results for pure PEO and PEO-CdS nanocomposites with different inorganic content

CdS wt% in PEO	$T_m \pm \sigma_N$/°C	$\Delta H_m \pm \sigma_N$/J g^{-1}	$T_c \pm \sigma_N$/°C	$\Delta H_c \pm \sigma_N$/J g^{-1}
0	64.7±1.2	150±7	48.5±0.9	141±5
1.8	64.5±0.5	137±12	43.2±0.5	132±10
2.6	64.5±0.7	145±8	42.5±0.5	124±9
3.4	62.7±1.1	142±8	38.7±0.8	126±9

T_m Melting peak temperature, ΔH_m specific enthalpy of melting, T_c crystallization peak temperature, ΔH_c specific enthalpy of crystallization, σ_N standard deviation

can take place because of the aliphatic periphery of the TOPO layer and because of the presence of sulfur vacancies (indicated by the low intensity bands in the emission spectrum in Fig. 2). This means that, at the nanoparticle surfaces, there is an excess of ruptures in the CdS crystal lattice, with unsaturated Cd ions bearing a partially positive charge. This will strongly affect the distribution of the torsional C–O–C–C angles due to Coulomb interaction as was indicated above. It is worth mentioning that the other PEO nanocomposite systems showed a somewhat different behavior. Introduction of functionalized single-wall nanotubes significantly reduced the melting temperature of PEO, although, as in our case, it did not affect the crystallinity to a high extent [42]. On the other hand, NiO nanoparticles in an NH_2 terminated PEO induced complete diminishing of the matrix melting peak [40]. In line with these findings, it should be emphasized that the observed crystallization and/or melting behaviour of PEO is atypical, compared to some other semicrystalline polymers where nanofillers promote crystallization of the matrix. For example, in our previous paper on polyvinyl alcohol (PVA)-PbS nanocomposites [27], it was found that nanoparticles acted as nucleation agents and shifted the onset of crystallization of PVA by more than 10 °C towards higher temperature. Similar results were also obtained in the case of MMT-filled PVA [50], polypropylene [51] and nylon-6 [52].

Figure 7 shows the TGA curves of pure PEO and PEO-CdS nanocomposites. It can be seen that the introduction of the CdS nanoparticles improves the thermal stability of the matrix. The nanocomposite with 3.4 wt% of inorganic phase has an onset temperature of decomposition of about 25 °C higher than that of pure PEO. A possible reason for this behaviour could be the slower chain dynamics of the PEO chains in the vicinity of the particle surfaces suggested above. Thermal decomposition of polymers usually starts with scission of weak bonds, followed by chain-transfer reactions of the formed free radicals, which proceed until the whole material is affected. Obviously, restricted chain motions close to the TOPO-capped nanoparticle surfaces could slow down free-radical chain transfer to a certain extent and consequently improve the thermal stability of PEO (Fig. 7). This conclusion could be supported by previous studies on polystyrene-co-maleic acid (PS-co-MAc)-CdS [21] and polystyrene (PS)-CdS nanocomposites [20]. The significant improvement in thermal stability, observed for these two nanocomposites, was attributed to the highly restricted motions of the polymer chains due to their chemical interaction with the sulfur at the surface of the CdS nanoparticles, which was established by Fourier transform infrared (FTIR) spectroscopy. FTIR analyses did not reveal any difference between the spectra of pure PEO and PEO-CdS nanocomposites (and therefore the spectra will not be reported). Weaker interaction between the inorganic and organic phases in this case could be responsible for the modest influence of the CdS nanoparticles on the thermal stability of PEO, compared to that noticed for PS-co-MAc and PS. It is important to mention that the TGA analyses showed that the as-obtained PEO powder had a lower thermal stability than the PEO film. This indicates that preparation of the films (probably residual solvent) also had an influence on the reported results. However, all the samples were prepared in the exactly same manner, and this should not affect the former discussion.

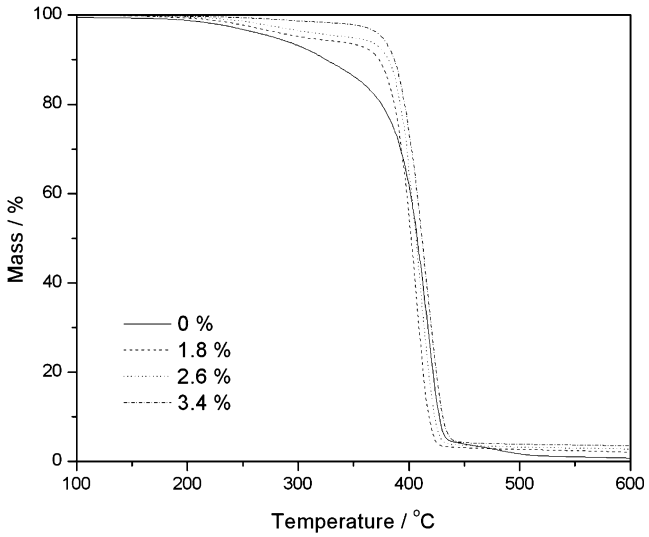

Fig. 7 TGA curves of pure PEO and PEO-CdS nanocomposites obtained at a heating rate of 10 °C min^{-1}

Conclusions

CdS nanoparticles were synthesized using a cadmium(II) complex of thiocarbohydrazide as the precursor. Their sizes varied depending on the time intervals at which they were isolated from the reaction mixture. CdS nanoparticles isolated after 45 min were used for the preparation of PEO-CdS nanocomposites with different inorganic phase contents. Optical measurements of the water solution of the nanocomposite showed a blue-shifted absorption onset with respect to bulk CdS and a pronounced band-to-band recombination. TEM analysis revealed that the nanoparticles are well dispersed in the polymer matrix. Introduction of nanostructured CdS led to a hindered crystallization of PEO due conformational changes of the polymer chains in the vicinity of the particle surfaces. It was found that the crystallization temperature of the host matrix decreased with increasing CdS content. At the same time, its melting temperature and crystallinity were not significantly affected by the presence of the nanoparticles. TGA measurements showed that the CdS nanoparticles improved the thermal stability of the PEO. In the case of the nanocomposite with 3.4 wt% of inorganic content, the onset of thermal decomposition was shifted to a higher temperature by about 25 °C.

References

1. Godovsky DY (2000) Advan Polym Sci 165:153
2. Ghosh PK, Maity R, Chattopadhyay KK (2005) J Nanosci Nanotech 5:300
3. Gorelikov I, Kumacheva E (2004) Chem Mater 16:4122
4. Bekiari V, Pagonis K, Bokias G, Lianos P (2004) Langmuir 20:7972
5. Yu S-H, Yoshimura M, Moreno JMC, Fujiwara T, Fujino T, Teranishi R (2001) Langmuir 17:1700
6. Khanna PK, Lonkar SP, Subbarao VVVS, Jun K-W (2004) Mater Chem Phys 87:49
7. Tamborra M, Striccoli M, Comparelli R, Curri ML, Petrella A, Agostiano A (2004) Nanotechnology 15:240
8. Chen M, Xie Y, Qiao Z, Zhu Y, Qian Y (2000) J Mater Chem 10:329
9. Du H, Xu GQ, Chin WS, Huang L, Ji W (2002) Chem Mater 14:4473
10. Moffitt M, McMahon L, Pessel V, Eisenberg A (1995) Chem Mater 7:1185
11. Lin J, Cates E, Bianconi PA (1994) J Am Chem Soc 116:4738
12. Antolini F, Pentimalli M, Di Luccio T, Terzi R, Schioppa M, Re M, Mirenghi L, Tapfer L (2005) Mater Lett 59:3181
13. Bekiari W, Lianos P (2000) Langmuir 16:3561
14. Peng Q, Zhai J, Wang W, Yan X, Bai F (2003) Cryst Growth Des 3:623
15. Choudhury KR, Samoc M, Petra A, Prasad PN (2004) J Phys Chem B 108:1556
16. Hilinski EF, Lukas PA, Wang Y (1988) J Chem Phys 89:3435
17. Zhang J, Coombs N, Kumacheva E (2002) J Am Chem Soc 124:14512
18. Godovsky DYu, Varfolomeev AE, Zaretsky DF, Nayana Chandrakanthi RL, Kündig A, Weder C, Caseri W (2001) J Mater Chem 11:2465
19. Yeh W, Wei K-H (2003) Macromolecules 36:7903
20. Šajinović D, Šaponjić ZV, Cvjetićanin N, Marinović-Cincović M, Nedeljković JM (2000) Chem Phys Lett 329:168
21. Nair PS, Radhakrishnan T, Revaprasadu N, Kolawole GA, Luyt AS, Djoković V (2005) J Phys Chem Solid 66:1302
22. Liu Y, Chen L, Su B, Huang A, Hua J, Sang W, Min J, Meng Z (2002) J Appl Polym Sci 84:1263
23. Radhakrishnan T, Georges MK, Nair PS, Luyt AS, Djokovic V (2007) J Nanosci Nanotech 7:986
24. Nair PS, Radhakrishnan T, Revaprasadu N, Kolawole GA, Luyt AS, Djoković V (2005) Appl Phys A Mater Sci Proces 81:835
25. Nair PS, Radhakrishnan T, Revaprasadu N, van Sittert CGCE, Djoković V, Luyt AS (2004) Mater Lett 58:361
26. Djoković V, Nedeljković JM (2000) Macromol Rapid Commun 21:994
27. Kuljanin J, Čomor MI, Djoković V, Nedeljković JM (2006) Mater Chem Phys 95:67
28. Qiao Z, Xie Y, Chen M, Xu Y, Zhu Y, Qian Y (2000) Chem Phys Lett 321:504
29. Tessler N, Medvedev V, Kazes M, Kan S, Banin U (2002) Science 295:1506
30. Han M, Gao X, Su JZ, Nie S (2001) Nat Biotechnol 19:631
31. Murray CB, Noms DJ, Bawendi MG (1993) J Am Chem Soc 115:8706
32. Peng XG, Manna L, Yang WD, Wickham J, Scher E, Kadavanich A, Alivisatos AP (2000) Nature 404:59
33. Peng ZA, Peng X (2001) J Am Chem Soc 123:183
34. Bunge SD, Krueger KM, Boyle TJ, Rodriguez MA, Headley TJ, Colvi VL (2003) J Mater Chem 13:1705
35. Nair PS, Radhakrishnan T, Revaprasadu N, Kolawole GA, O'Brien P (2002) Chem Commun 6:564
36. Capuano F, Croce F, Scrosati B (1991) J Electrochem Soc 138:1918
37. Alcantar NA, Aydil ES, Israelachvili JN (2000) J Biomed Mater Res 51:343
38. Strawhecker KE, Manias E (2003) Chem Mater 15:844
39. Chen H-W, Chang F-C (2001) Polymer 42:9763
40. Deki S, Yanagimoto H, Hiraoka S, Akamatsu K, Gotoh K (2003) Chem Mater 15:4916
41. Deki S, Sayo K, Yamada A, Akamatsu K, Hayashi S (1999) J Coll Interf Sci 214:123
42. Geng HZ, Rosen R, Zheng B, Shimoda H, Fleming L, Liu J, Zhou O (2002) Adv Mat 14:1387
43. Zhang Q, Archer LA (2002) Langmuir 18:10435
44. Xiong H-M, Zhao X, Chen J-S (2001) J Phys Chem B 105:10169
45. Caseri W (2000) Macromol Rapid Commun 21:705
46. Brus L (1984) J Chem Phys 80:4403
47. Rajh T, Mićić OI, Lawless D, Serpone N (1992) J Phys Chem 96:4633
48. Wang Y, Suna A, McHugh J, Hilinski EF, Lukas PA, Johnson RD (1990) J Chem Phys 92:6927
49. Borodin O, Smith GD, Bandyopadhyaya R, Byutner O (2003) Macromolecules 36:7873
50. Strawhecker KE, Manias E (2000) Chem Mater 12:2943
51. Manias E, Touny A, Wu L, Strawhecker K, Lu B, Chung TC (2001) Chem Mater 12:3516
52. Lincoln DM, Vaia RA, Wang Z-G, Hsiao BS, Krishnamoorti R (2001) Polymer 42:9975